NANO LETTERS

Letter

pubs.acs.org/NanoLett

Direct Measurement of Coherency Limits for Strain Relaxation in Heteroepitaxial Core/Shell Nanowires

Shadi A. Dayeh,*[,†,‡] Wei Tang,[§] Francesca Boioli,[∥] Karen L. Kavanagh,[⊥] He Zheng,[#] Jian Wang,[▽] Nathan H. Mack,[○] Greg Swadener,[△] Jian Yu Huang,[¶] Leo Miglio,[∥] King-Ning Tu,[§] and S. Tom Picraux[†]

[†]Center for Integrated Nanotechnologies, Los Alamos National Laboratory, P.O. Box 1663, K771 Los Alamos, New Mexico 87545, United States

[‡]Department of Electrical and Computer Engineering, University of California, San Diego, La Jolla, California 92093, United States

[§]Department of Materials Science, University of California, Los Angeles, Engineering V Building, Los Angeles, California 90095, United States

[∥]Department of Materials Science, University of Milano-Bicocca, Milano, Italy

[⊥]Department of Physics, Simon Fraser University, 8888 University Dr., Burnaby, BC, V5A 1S6 Canada

[#]School of Physics and Technology, Center for Electron Microscopy and MOE Key Laboratory of Artificial Micro- and Nano-structures, Wuhan University, Wuhan 430072, China

[▽]Physical Chemistry and Applied Spectroscopy, Los Alamos National Laboratory, P.O. Box 1663, K771 Los Alamos, New Mexico 87545, United States

[○]Material Science and Technology Division, Los Alamos National Laboratory, P.O. Box 1663, K771, Los Alamos, New Mexico 87545, United States

[△]Mechanical Engineering and Design Department, Aston University, Birmingham B4 7ET, United Kingdom

[¶]Center for Integrated Nanotechnologies, Sandia National Laboratories, MS 1303, Albuquerque, New Mexico 87185, United States

Supporting Information

ABSTRACT: The growth of heteroepitaxially strained semiconductors at the nanoscale enables tailoring of material properties for enhanced device performance. For core/shell nanowires (NWs), theoretical predictions of the coherency limits and the implications they carry remain uncertain without proper identification of the mechanisms by which strains relax. We present here for the Ge/Si core/shell NW system the first experimental measurement of critical shell thickness for strain relaxation in a semiconductor NW heterostructure and the identification of the relaxation mechanisms. Axial and tangential strain relief is initiated by the formation of periodic $a/2$ ⟨110⟩ perfect dislocations via nucleation and glide on {111} slip-planes. Glide of dislocation segments is directly confirmed by real-time in situ transmission electron microscope observations and by dislocation dynamics simulations. Further shell growth leads to roughening and grain formation which provides additional strain relief. As a consequence of core/shell strain sharing in NWs, a 16 nm radius Ge NW with a 3 nm Si shell is shown to accommodate 3% coherent strain at equilibrium, a factor of 3 increase over the 1 nm equilibrium critical thickness for planar Si/Ge heteroepitaxial growth.

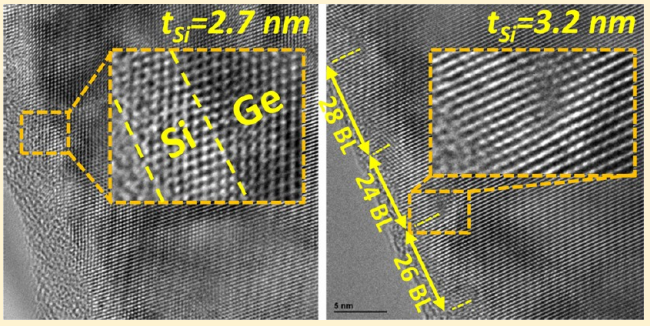

KEYWORDS: *Heterostructure, core/shell, nanowire, critical thickness, germanium, silicon*

Advanced device architectures for electronic and optoelectronic applications often require heterostructures to optimize performance.[1−9] Strain engineering in these heterostructures has proven to be a critical strategy in tailoring the energy band-edge properties for enhanced charge carrier transport[10,11] and photoemission properties.[12] In current planar technology essentially all high performance Si-based microprocessors and III−V semiconductor lasers incorporate strain to enhance their performance. Dislocation-free heterostructures, however, cannot be grown with arbitrary thickness before the strain energy in the structure exceeds that required to form dislocations and defects in the grown layer, which in turn degrade its properties.[13] To increase this critical thickness to be more useful for device applications, it is of interest to grow on compliant substrates or on 3-dimensional structures where the

Received: June 14, 2012
Revised: September 25, 2012

   dx.doi.org/10.1021/nl3022434 | *Nano Lett.* XXXX, XXX, XXX−XXX

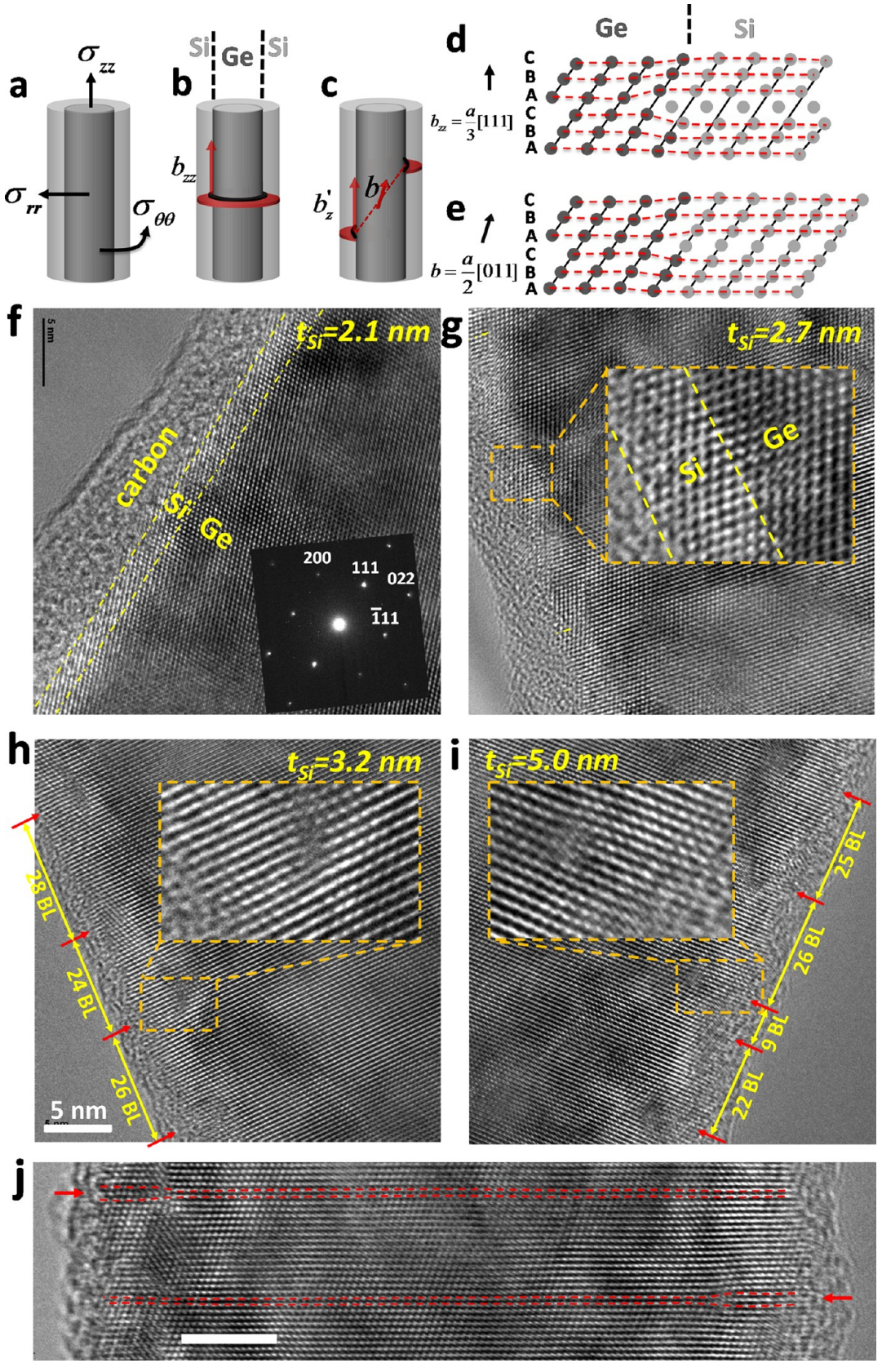

Figure 1. (a) Schematic diagram illustrating the different stresses existing in a core/shell NW: σ_{zz}, axial stress, σ_{rr}, radial stress, and $\sigma_{\theta\theta}$, tangential stress. (b) Schematic diagram depicting axial strain relief with a Frank partial dislocation at the interface with Burgers vector $b_{zz} = a/3$ [111]. The effect of this dislocation is the appearance of an extra (111) plane in the Si shell along a single cross-section of the wire. (c) Schematic diagram depicting axial strain relief from a Burgers vector $b = a/2$ [011]. The projection of this Burger's vector along the growth axis is $b_z' = a/3$[111], resulting in the same formation of an extra (111) plane in the Si shell with respect to the core via bond shifting at the interface. Atomic arrangement (d) for a partial dislocation segment and (e) for a perfect dislocation segment. (f–i) Same magnification HRTEM images of a 15 nm radius Ge core

dx.doi.org/10.1021/nl3022434 | *Nano Lett.* XXXX, XXX, XXX–XXX

Figure 1. continued

with different Si shell thicknesses imaged from a ⟨110⟩ zone axis. (f) 2.1 nm thick Si shell with corresponding selective area diffraction pattern showing a single crystal core−shell structure with [111] growth axis. The outermost carbon shell develops during electron beam irradiation in TEM. (g) 2.7 nm thick Si shell case. The inset is a magnified view at the Ge/Si interface. (h) 3.2 nm thick Si shell with a relative periodic pattern of extra (111) planes in the Si shell, where the number of (111) bilayers (BL) between these extra (111) planes is indicated. The inset is a magnified image at the Ge/Si interface showing the extra (111) plane in the Si shell. (i) 5 nm thick Si shell with similar periodicity of the extra (111) planes as in h. (j) HRTEM image showing that the dislocations observed in h and i do not exist in a single cross-section and therefore are not Frank dislocations. Scale bar is 5 nm.

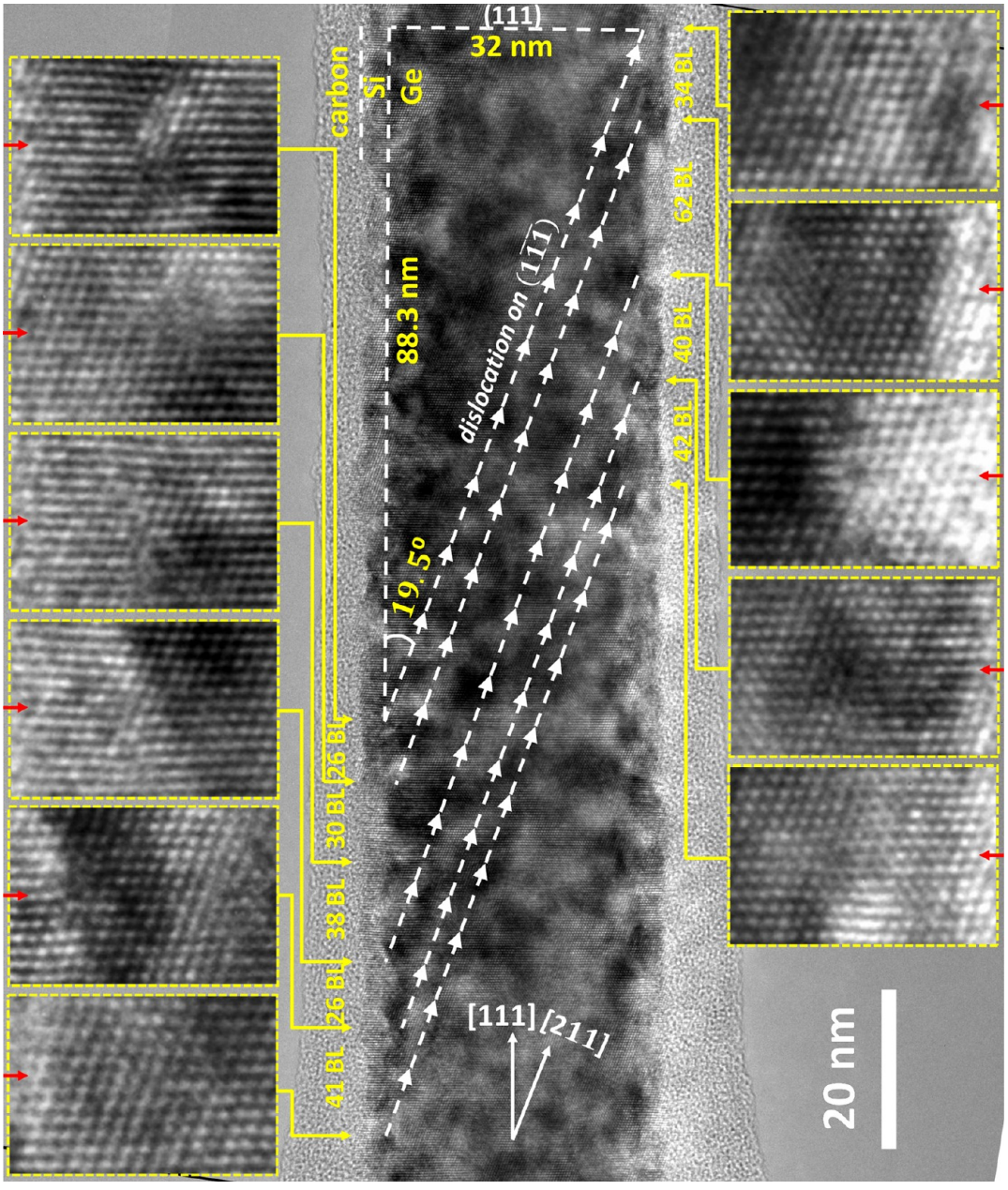

Figure 2. HRTEM sideview image (beam direction [01$\bar{1}$]) of a Ge/Si core/shell NW over a sufficient axial distance to observe dislocation segments formed by glide along the circumference of the NW. The insets are enlarged portions from the same image indicating the locations of extra Si (111) planes. $a/2$[011] perfect dislocation segments nucleate at the surface of the NW and glide on the (1$\bar{1}\bar{1}$) plane on a single {112} facet. Successive nucleation of three such dislocation segments can lead to the formation of complete loops around the Ge core. Five such loops are observed in this HRTEM image.

misfit strain can be shared between the heterostructured layers.[14]

Semiconductor core/shell nanowires (NWs) offer an ideal platform for such heterostructuring where the small NW core diameters[15] provide the required "substrate" compliance and where heterointerfaces are abrupt.[16] However, 10 years after the first demonstration of core/shell NW growth,[16] there is still no experimental quantification of their critical dimensions and

dx.doi.org/10.1021/nl3022434 | *Nano Lett.* XXXX, XXX, XXX−XXX

no clear identification of the mechanisms by which they relax, despite a number of theoretical predictions[17−21] on their coherency limits. This contrasts to strained-layer growth on planar substrates where mechanisms and critical dimensions are well-established.[22] Here using Ge/Si core/shell NWs, we provide: (i) the first experimental measurement of the critical thicknesses for strain relief via dislocations, (ii) the operative strain relaxation mechanism by observing periodically spaced $a/2$ ⟨110⟩ perfect dislocation loop segments in a single NW, (iii) dislocation dynamics simulations describing the dislocation segment nucleation and propagation on faceted core/shell NWs, and (iv) in situ transmission electron microscope (TEM) observation of the thermally induced dislocation segment glide in core/shell NWs.

In a heteroepitaixal core/shell cylindrical system, there exist three different stresses at the heterointerface (Figure 1a): (i) along the axis of the NW, σ_{zz}, (ii) along the radius of the NW, σ_{rr}, and (iii) along the tangential direction to the NW, $\sigma_{\theta\theta}$. Previous works have considered Frank-type dislocations (Figure 1b,d) as one possible source of strain relief in core/shell heterostructured NWs.[17−21] There are many examples of pure edge dislocations detected in NW heterostructures.[23−25] However, such dislocations are unlikely to form by low energy glide processes, at least at the typical growth and annealing temperatures (<600 °C) for our core/shell NWs. Their Burgers vectors do not sit on a low energy glissile plane, and thus, propagation by glide is energetically unfavorable. In contrast, perfect dislocations (Figure 1c,e), which form by loop nucleation and glide on one of the {111} slip planes, can be formed at our growth temperatures (∼ 500 °C). Reactions of two such dislocations have been used to explain the existence of these sessile dislocation segments.[26] Here, we will establish the nature of the dislocation formation as the coherency limit is reached.

Our experimental approach consisted of growing ⟨111⟩ oriented Ge NW cores by chemical vapor deposition through the vapor−liquid−solid growth mechanism with subsequent in situ Si shell deposition.[27] The Ge NW core radii were 15 nm, and the Si shell thickness was varied from 1 to 10 nm (see Figure 1). Postannealing at 600 °C was carried out for evaluation of the equilibrium critical thickness. As the shell thickness increases to 2.7 nm (Figure 1f,g), we generally found perfect coherent epitaxial core/shell structures without defects. At a thickness of 3.2 nm (Figure 1h) up to 5 nm (Figure 1i), we began to observe additional strain relieving Si (111) planes with respect to the Ge core, along the growth axis of the NW that had a projected component of the Burgers vector of $a/3[111]$ (b'_z in Figure 1b). The average axial separation of these additional planes was 26 (111) bilayers or 8.5 nm. From basic elasticity theory, the linear density of dislocations necessary to relieve stress in the axial direction is $\rho = f/|b\cos(\theta)|$, where $|b|$ is the magnitude of the dislocation Burgers vector projected on the plane of the heterointerface, θ is the angle between the Burgers vector and the growth orientation, and $f = 0.0419$ is the lattice mismatch of Si with respect to Ge. For a perfect dislocation, perpendicular to the [111] NW axis, with an $a/2$ ⟨110⟩ Burgers vector component projected on the [111] growth orientation equal to b'_z, this results in an axial dislocation separation distance, $s = 1/\rho = 7.5$ nm, 12% less but consistent with our observed dislocation spacing (8.5 nm) accounting for partial relaxation of the σ_{zz} and $\sigma_{\theta\theta}$ strains. From Figure 1, we conclude that the equilibrium critical Si shell thickness is 3 nm for a 15 nm Ge core radius which significantly exceeds that of bulk heteroepitaxy (1 nm). It is expected that additional reduction in the Ge NW core radius can further increase the equilibrium critical thickness.[17−21]

For [111] oriented NWs, there are three {111} slip planes {$(1\bar{1}\bar{1})$, $(\bar{1}11)$, $(\bar{1}1\bar{1})$} at angles of 19.5° from the growth axis. When Ge/Si NWs are viewed along a ⟨110⟩ zone axis in the TEM, $a/2$ ⟨110⟩ dislocation segments in the Si shell on one of these slip planes should be observable. A dislocation could nucleate on one edge of the NW and move in its slip plane by glide to deposit a misfit line at the Si/Ge interface. Figure 2 shows several instances of these dislocations that nucleate on one surface of the Si shell and glide on the $(\bar{1}\bar{1}1)$ plane. Dislocations of the same type could successively nucleate on three adjacent facets leading to a complete loop formation around the NW core. For a 16 nm NW radius, the axial loop length is $32/\tan(19.5°)$ nm = 90 nm, consistent with the 88 nm observed experimentally in Figure 2. Interestingly, five such dislocation loops could be traced from one surface of the NW along the $(1\bar{1}\bar{1})$ plane to the other surface (Figure 2). It is also evident from the magnified images in Figure 2 that these are perfect dislocation segments. In addition, in all growths and TEM characterization of this study, we never observed extra Si planes on both surfaces of the Si shell on the same (111) plane orthogonal to the growth direction (see Figure 1j), which further confirms that these dislocations are not Frank dislocations. Thus, these observations show that the strain relieving mechanism for loss of coherency in ⟨111⟩ oriented Ge/Si core/shell NWs is by dislocation glide on the inclined {111} planes.

To further elucidate the formation and propagation mechanism of perfect dislocations by glide and to identify the preferred nucleation sites and dislocation line directions, we first analyzed the heteroepitaxial stress field in a simplified ⟨111⟩ oriented Ge/Si core/shell NW geometry with {112} or {110} side facets. The core radius and the shell thickness were set equal to 32 and 6 nm, to exceed the measured critical thickness. In Figure 3a and b, we plot the resolved shear stress (RSS), calculated by the finite element method, for a dislocation with $(\bar{1}11)$ slip plane and $b = a_{Si}/2$ [110] Burgers vector, in a NW with {112} and {110} side facets, respectively. A large positive value of the RSS indicates a preferred site for dislocation nucleation and propagation. On the contrary, in case of zero or negative RSS the propagation of the same dislocation is hindered. By inspecting the RSS map in Figure 3 we expect dislocations to nucleate at the NW corners where the RSS is maximum and to propagate in the Si shell volume where the RSS is positive.

To support this analysis, dislocation dynamics (DD) simulations[28,29] were performed in the two NW configurations described above. In Figure 3e ({112 facets case) and Figure 3f ({110} facets case) we show two snapshots from the simulations obtained by considering dislocations with $(\bar{1}11)$ slip plane and $b = a_{Si}/2[110]$ Burgers vector. In agreement with the RSS analysis and prior experimental observations,[30] we found that the nucleation of dislocations is preferential to the NW corners, as shown in Figure 3e where a small new loop is located at the NW edge position. Moreover, dislocations evolve from the NW corners in their slip plane, sweeping across the area in the Si shell where the RSS is positive, and depositing a misfit line at the Ge/Si interface. As a consequence, we observed some straight dislocation lines crossing a single NW facet, as in Figure 3f, or dislocation segments that cross a NW corner depositing a misfit line on two adjacent facets, as in

dx.doi.org/10.1021/nl3022434 | Nano Lett. XXXX, XXX, XXX−XXX

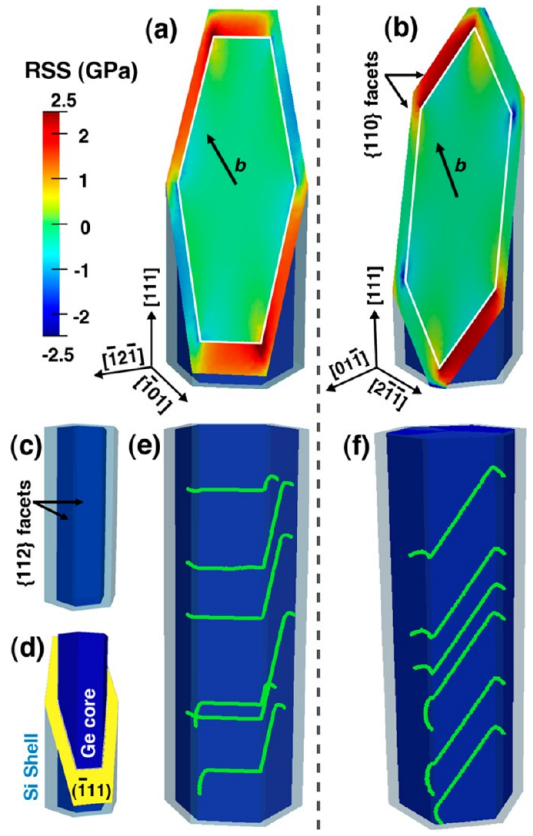

Figure 3. (a,b) Resolved shear stress (RSS) variation in a ($\bar{1}$11) plane crossing a [111] oriented NW with {112} facets in a and {110} facets in b for the [011]-($\bar{1}$11) slip system. Positive RSS values favor dislocation nucleation and glide. (c) A diagram of the NW geometry with {112} facets and (d) a drawing of the ($\bar{1}$11) glide plane intersecting the Si shell. (e,f) Dislocation line positions obtained by dislocation dynamics simulations through inserting small dislocation loops in the Si shell volume for {112} facets in e and {110} facets in f.

Figure 3e. Dislocation lines perpendicular to the NW growth axis, as shown in Figure 3e, have a projected component of the Burgers vector $b_{z'} = a/3[111]$, and the position of the extra half-plane in the Si shell connected with such dislocation geometry is aligned to the [211] direction, in excellent agreement with the experimental observations. These dislocation segments will relieve the maximum axial strain, while the oblique segments can relax the tangential strain. Dislocation evolution in the other slip planes {($1\bar{1}1$) and ($11\bar{1}$)} (not shown) led to similar dislocation line arrangements in the adjacent NW facets, that contribute to axial and tangential strain relaxation in the whole Si volume. Moreover, no propagation of loops in the basal (111) plane was ever observed, as for Frank-type dislocations, according to RSS predictions. These results corroborates the experimental findings of gliding dislocations observed in Figures 1 and 2 and shed light on their nucleation sites, propagation, and termination in the Si volume.

Our in situ grown single crystal core/shell NWs already show dislocation segments in the as-grown NWs with Si shell thicknesses above 3 nm, even without postannealing. The 600 °C annealing step allowed us to observe the periodicity of these dislocations as shown in Figures 1 and 2. To further confirm dislocation glide on the ($1\bar{1}\bar{1}$) planes, we performed in situ TEM experiments on as-grown NWs where the temperature of the TEM stage was ramped (5 °C/s) to 450 °C, paused for 30 min, and then ramped to 600 °C. Careful inspection of video frames taken during the annealing experiments showed that dislocation movement and glide occurs on the ($1\bar{1}\bar{1}$) planes.

Figure 4a–d shows HRTEM snapshots at a short incremental time with two reference points marked by arrows

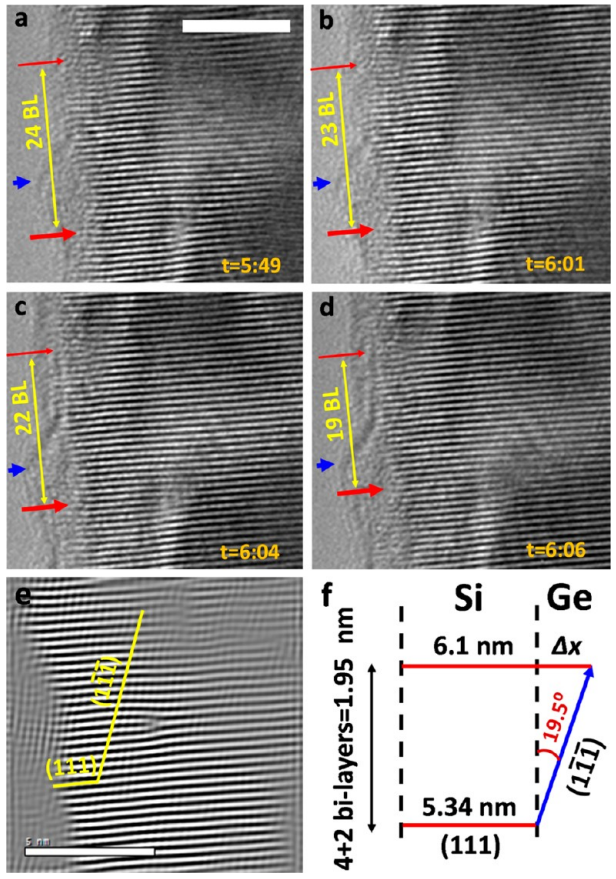

Figure 4. (a–d) HRTEM sideview cross-section snapshots from a recorded video of dislocation loop movement on a($1\bar{1}\bar{1}$) plane. The thin red arrow is a reference marker of a fixed-position extra Si (111) plane, and the blue arrow is a reference marker at the corner of a carbon-coated shell during TEM exposure. The thick red arrow points at the extra Si (111) plane that is moving closer to both references. The scale bar is 5 nm. Time, *t*, is given in each frame in min:s. (e) Inverse FFT of the image in c showing contrast from both (111) and ($1\bar{1}\bar{1}$) planes. (f) Geometrical relationship for expansion of the extra Si (111) plane during gliding on the ($1\bar{1}\bar{1}$) Slip plane.

on the images a–d: a thin red arrow for a dislocation with small insertion of an extra (111) plane in the Si shell, and a blue arrow at the corner of the carbon-coated portion of the NW to reference the relative position along the NW. The extra (111) Si plane due to the dislocation and whose position with respect to the reference markers was monitored is marked by the thick red arrow. Initially, the separation between the two dislocation loops (two red arrows) was 24 bilayers, and this reduced to 19 bilayers within 17 s (Figure 4a,b). Inverse FFT of these images indicates a ⟨110⟩ beam condition over which the ($1\bar{1}\bar{1}$) plane position can be verified (Figure 4e). The expansion of the extra (111) plane is governed by the simple geometric relation in Figure 4f given by $\Delta x = \tan(19.5°) \times 1.95$ nm = 0.7 nm, where 1.95 nm is the axial dislocation movement in the [111] direction. The measured distance between the extra Si (111) planes in Figure 3a,b is 0.76 nm, which is in good agreement

dx.doi.org/10.1021/nl3022434 | *Nano Lett.* XXXX, XXX, XXX–XXX

with the expected value from Figure 4f. The glide velocity during the motion of these dislocations is 0.13 nm/s which is 10^4 times slower than the glide velocity in $Si_{0.77}Ge_{0.23}$/Si thin film heterostructures at the same temperature,[31] enabling us to observe and accurately measure dislocation extension at a subnanometer scale.

The discussion above points to a critical thickness in core/shell NWs to partially relieve strain. Cross-sectional HRTEM (Figure 5a) for a Si shell thickness >3 nm showed extra (111) planes along the cross-section of the nanowire. Dislocation segments on all three slip planes lead to extra {111} planes in the Si shell that can be observed only when looking at an axial cross-section of the heterostructured NW as is the case in Figure 5a. The resulting extra Si {111} planes in the cross-section of the heterostructured NW allows for tangential strain relief along the circumference of the NW.

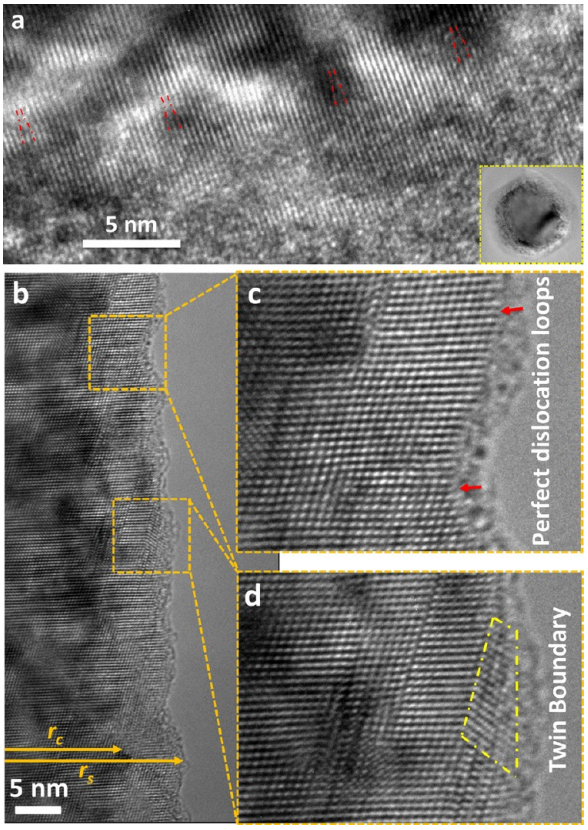

Figure 5. (a) Axial HRTEM cross-section of a Ge/Si core/shell NW with a 3.5 nm thick Si shell viewed from slightly off a NW ⟨111⟩ growth axis (⟨332⟩ zone view) showing semiperiodic extra {111} planes in the Si shell with an average spacing of 8 nm. (b) HRTEM sideview cross sections of a Ge/Si core/shell NW with r_c = 15 nm and r_s = 23 nm (8 nm shell thickness) showing an onset of a roughened Si shell on the Ge NW. Higher magnification images showing in c the existence of perfect dislocation loops and (d) formation of twin boundaries.

As the Si shell thickness increases to 8 nm on a 15 nm Ge core radius (Figure 5b), we start to observe additional strain-relieving mechanisms. Figure 5c and 5d show roughening and twin boundary formation (Figure 5c) in addition to the perfect dislocation segments (Figure 5c). Tilt twin boundaries in the thick Si shells can result from rearrangement of excess dislocation segments as the Si shell layer thickness increases and roughens, which in turn helps in relieving residual axial and tangential strain not relieved by the perfect dislocations discussed above. The analysis of axial strain based on FFT patterns from Figure 5b indicates essentially full axial strain relief, whereas similar analysis for shell thicknesses in the range of 1−4 nm gave up to ∼3% residual axial strain even with the insertion of the perfect dislocation segments, which corroborates with the RSS analysis discussed in Figure 3.

The present results for thicker shells are consistent with earlier core/shell NW studies. In our case, high quality core−shell growth is enabled by a procedure that we devised to engineer a Si blocking interface between the Au seed and the Ge NW sidewalls.[32] This approach leads to the elimination of Au diffusion during the synthesis of single-crystal Ge/Si core/shell NW heterostructures which enhances early roughening during shell growth. The present growth sequence enables a better assessment of coherency limits and relaxation mechanisms in core/shell NWs. In contrast to earlier reports on strain relaxation in Ge/Si core/shell NWs, where ex-situ Au etching was performed prior to the epitaxial growth of the Si shells at higher temperatures than those used here,[23] strain relaxation via island growth was not observed in our experiments. For [110] oriented NWs, indications of $a/2$[110] dislocation loops were observed,[33] which is consistent with our findings for misfit strain relaxation, and which we also find to be the case upon close examination of the TEM images of the first report on synthesis of Ge/Si core/shell NWs.[16] Rotation in FFT patterns of a Ge/Si HRTEM image in a recent report indicates twin and grain boundary formation when the Si shells becomes sufficiently thick,[34] which is in accordance with our observations for thick Si shells. It is worth noting that the Ge/Si material system provides a simpler platform for studying strain relief in core/shell heterostructured NWs when compared to III/V counterparts, where it has been observed that shell growth in such systems depends on the polarity of the faceted surfaces. This effect can lead, for example, to shell thicknesses that are not uniform across the cross-section of a single InAs/GaAs core/shell structures.[35]

These observations provide a framework for understanding strain relaxation in 3-dimensional nanostructures. In particular, we have identified the coherency limits for core/shell NWs for the first time and determined the operational dislocation glide mechanism which limits coherency. For some material systems such as III−V NWs, the perfect dislocation loop segments can lead to different magnitudes of axial and radial strain relief, where it becomes conceivable to tailor axial and tangential stresses separately. The implication of such strain engineering would, for example, allow tailoring the stress components along a transistor's channel length, when made on a heterostructured core/shell NW, for separate tuning of electron and hole mobilities. Also, thicknesses of shells must be carefully controlled since increasing strain can enhance mobility while maintaining thin shell thicknesses to achieve high gate capacitance and therefore high transistor drive currents and switching speeds.

Experimental Section. Ge NWs were grown on Ge (111) surfaces in a cold wall CVD system using 30 nm diameter Au colloids according to the preparation and two-step growth (90 s nucleation step at 360 °C followed by quick ramp to 276 °C) procedures, as described elsewhere.[36] After the NW elongation step at 276 °C in GeH_4 (30% in H_2) and GeH_4 partial pressure, P_{GeH_4} = 0.6 Torr, a SiH_4 (50% in H_2) flow was implemented for 15−30 min (P_{SiH_4} = 1.75 Torr) to deposit a Si interfacial barrier

dx.doi.org/10.1021/nl3022434 | Nano Lett. XXXX, XXX, XXX−XXX

layer underneath Au, whose thickness was on the order of the NW diameter. SiH_4 was then introduced, and the temperature was ramped up to 500 °C where the i-Si shell deposition took place at P_{SiH_4} = 0.25 Torr with a total ramp and deposition times of 17−53 min. The grown samples were annealed at 600 °C in a rapid thermal annealing system for 30 min under forming gas (15% H_2 in N_2).

For transmission electron microscopy (TEM), the as-grown NWs were suspended in an isopropanol solution and deposited on lacey carbon TEM grids. Investigations were carried out with a TEM with a field emission electron source operating at an accelerating voltage of 300 kV. The in situ TEM studies were performed with a heating stage capable of heating up to 1000 °C. For cross-sectional TEM, the NWs were transferred directly from the growth substrate by dry transfer onto a 50 μm thick fluoropolymer embedding film. The fluoropolymer film was then embedded into an Araldite based epoxy resin, and the whole structure was cut into 50−70 nm slices using a diamond ultramicrotome knife and transferred onto Cu grids for imaging.

Simulations. The epitaxial stress field in ⟨111⟩ oriented Ge/Si core/shell NWs with {112} or {110} side facets was calculated by using isotropic linear elasticity theory solved by the finite element method (FEM). The resolved shear stress (RSS) for a given dislocation type (defined by slip plane and Burgers vector) is the stress resolved in its slip plane with normal $\hat{n}$ along the Burgers vector direction b(RSS = $b\cdot\sigma\hat{n}$). This quantity shows the effective stress that drives the dislocation nucleation and glide motion.

Dislocation dynamics simulations employing the open-source code microMegas[37] were performed following a similar approach to the one proposed for nanoislands in ref 38. First, the coherent stress field of the NW, calculated by FEM, is applied as an external load in the simulations. Second, the dislocation-surface interaction is approximated by using a line-tension expression modified with respect to the typical bulk expression to mimic the force acting on segments touching the free surfaces.[38,39] Finally, the dynamics are solved by taking into account these two contributions and the stress field arising from all the dislocations in the NW volume. In the DD simulations presented here, dislocation loops with 4 nm radii are periodically introduced at random positions in the Si shell, similarly to ref 40. If the stress field at these positions promotes loop expansion, they will evolve with time and contribute to the NW strain relaxation.

■ ASSOCIATED CONTENT

Supporting Information

Movie recorded during in situ heating experiment and imaging of dislocation gliding as well as movies showing results from the dislocation dynamics simulations for dislocation nucleation, propagation, and termination in the cases of {112} and {110} facets. This material is available free of charge via the Internet at http://pubs.acs.org.

■ AUTHOR INFORMATION

Corresponding Author

*E-mail: shadi@lanl.gov.

Notes

The authors declare no competing financial interest.

■ ACKNOWLEDGMENTS

This work was performed, in part, at the Center for Integrated Nanotechnologies, a U.S. Department of Energy, Office of Basic Energy Sciences user facility at Los Alamos National Laboratory (Contract DE-AC52-06NA25396) and Sandia National Laboratories (Contract DE-AC04-94AL85000). This work is funded in part by the Laboratory Directed Research and Development (LDRD) program at Los Alamos National Laboratory.

■ REFERENCES

(1) Lu, W.; Xiang, J.; Timko, B. P.; Wu, Y.; Lieber, C. M. One-Dimensional Hole Gas in Germanium/Silicon Nanowire Heterostructures. *Proc. Natl. Acad. Sci.* **2000**, *102*, 10046.

(2) Liang, G.; Xiang, J.; Kharche, N.; Klimeck, G.; Lieber, C. M.; Lundstrom, M. Performance Analysis of a Ge/Si Core/Shell Nanowire Field Effect Transistor. *Nano Lett.* **2007**, *7*, 642.

(3) Yang, L.; Musin, R. N.; Wang, X.-Q.; Chou, M. Y. Quantum Confinement Effect in Si/Ge core-shell Nanowires: First-Principles Calculations. *Phys. Rev. B* **2008**, *77*, 195325.

(4) Peköz, R.; Raty, J.-Y. From Bare Ge Nanowire to Ge/Si Core/Shell Nanowires: A First-Principles Study. *Phys. Rev. B* **2009**, *80*, 155432.

(5) Amato, M.; Palummo, M.; Ossicini, S. Reduced Quantum Confinement Effect and Electron-Hole Separation in SiGe Nanowires. *Phys. Rev. B* **2009**, *79*, 201302.

(6) Peng, X.; Logan, P. Electronic Properties of Strained Si/Ge Core/Shell Nanowires. *Appl. Phys. Lett.* **2010**, *96*, 143119.

(7) Hafez, W.; Snodgrass, W.; Feng, M. 12.5 nm base pseudomorphic heterojunction bipolar transistors achieving f_T = 710 GHz and f_{max} = 340 GHz. *Appl. Phys. Lett.* **2005**, *87*, 252109.

(8) Wojtczuk, S.; Chiu, P.; Zhang, X.; Derkacs, D.; Harris, C.; Pulver, D.; Timmons, M. InGaP/GaAs/InGaAs 41% Concentrator Cells Using Bi-facial Epi-growth. *35th IEEE Photovoltaic Specialists Conference (PVSC)*, June 20−25, 2010; pp 001259−001264.

(9) Dayeh, S. A. *Semicond. Sci. Technol.* **2010**, *25*, 024004.

(10) Lee, M. L.; Fitzgerald, E. A.; Bulsara, M. T.; Currie, M. T.; Lochtefeld, A. Strained Si, SiGe, and Ge channels for high-mobility metal-oxide-semiconductor field-effect transistors. *J. Appl. Phys.* **2005**, *97*, 011101.

(11) Nainani, A.; et al. Engineering of Strained III-V Heterostructures for High Hole Mobility. *IEEE Int. Elect. Dev. Meeting* **2009**, DOI: 10.1109/IEDM.2009.5424267.

(12) Sun, X.; Liu, J.; Kimerling, C.; Michel, J. Room-Temperature Direct Bandgap electroluminescence from Ge-on-Si light-emitting Diodes. *Opt. Lett.* **2009**, *34*, 1198.

(13) Ismail, K. Effect of Dislocations in Strained Si/SiGe on Electron Mobility. *J. Vac. Sci. Technol., B* **1996**, *14*, 2776.

(14) Mooney, P. M.; Cohen, G. M.; Chu, J. O.; Murray, C. E. Elastic Strain Relaxation in Free-Standing SiGe/Si Structures. *Appl. Phys. Lett.* **2004**, *84*, 1093.

(15) Wu, Y.; Cui, Y.; Huynh, L.; Barrelet, C. J.; Bell, C. B.; Lieber, C. M. Controlled Growth and Structures of Molecular-Scale Silicon Nanowires. *Nano Lett.* **2004**, *4*, 433. Dayeh, S. A.; Picraux, S. T. Direct Observation of Nanoscale Size Effects in Ge Semiconductor Nanowire Growth. *Nano Lett.* **2010**, *10*, 4032.

(16) Lauhon, L. J.; Gudiksen, M. S.; Wang, D.; Lieber, C. M. Epitaxial Core-shell and Core-multishell Nanowire Heterostructures. *Nature* **2002**, *420*, 57.

(17) Liang, Y.; Nix, W. D.; Griffin, P. B.; Plummer, J. D. Critical Thickness Enhancement of Epitaxial SiGe Films Grown on Small Structures. *J. Appl. Phys.* **2005**, *97*, 043519.

(18) Raychaudhuri, S.; Yu, E. T. Calculation of Critical Dimensions for Wurtzite and Cubic Zinc Blende Coaxial Nanowire Heterostructures. *J. Vac. Sci. Technol., B* **2006**, *24*, 2053.

(19) Schmidt, V.; McIntyre, P. C.; Gösele, U. Morphological Instability of Misfit-Strained Core-Shell Nanowires. *Phys. Rev. B* **2008**, *77*, 235302.
(20) Trammell, T. E.; Zhang, X.; Li, Y.; Chen, L.-Q.; Dickey, E. C. Equilibrium Strain-Energy Analysis of Coherently Strained Core-Shell Nanowires. *J. Cryst. Growth* **2008**, *310*, 3084.
(21) Colin, J. Prismatic Dislocation Loops in Strained Core-Shell Nanowire Heterostructures. *Phys. Rev. B* **2010**, *82*, 054118.
(22) Pearsall, T. P., Ed. *Strained-Layer Superlattices: Materials Science and Technology*, Vol. *33*; Academic Press: New York, 1991.
(23) Goldthorpe, I. A.; Marshall, A. F.; McIntyre, P. C. Synthesis and Strain Relaxation of Ge-Core/Si-Shell Nanowire Arrays. *Nano Lett.* **2008**, *8*, 4081.
(24) Kavanagh, K. L.; Salfi, J.; Savelyev, I.; Blumin, M.; Ruda, H. E. Transport and Strain Relaxation in Wurtzite InAs-GaAs core-shell Heterowires. *Appl. Phys. Lett.* **2011**, *98*, 152103.
(25) Kavanagh, K. L. Misfit Dislocations in Nanowire Heterostructures. *Semicond. Sci. Technol.* **2010**, *25*, 024006.
(26) Kavanagh, K. L.; Saveliev, I.; Blumin, M.; Swadener, G.; Ruda, H. E. Faster radial strain relaxation in InAs−GaAs core−shell heterowires. *J. Appl. Phys.* **2012**, *111*, 044301.
(27) Dayeh, S. A.; Gin, A. V.; Picraux, S. T. Advanced core/multi-shell Germanium/Silicon Nanowire Heterostructures: Morphology and Transport. *Appl. Phys. Lett.* **2011**, *98*, 163112.
(28) Devincre, B.; Madec, R.; Monnet, G.; Queyreau, S.; Gatti, R.; Kubin, L. In *Mechanics of Nano-objects*: Presses de l'Ecole des Mines de Paris: Paris, 2011; p 85.
(29) Groh, S.; Devincre, B.; Kubin, L.; Roos, A.; Feyel, F.; Chaboche, J.-L. *Philos. Mag. Lett.* **2003**, *83*, 303.
(30) Dayeh, S. A.; Wang, J.; Li, N.; Huang, J. Y.; Gin, A. V.; Picraux, S. T. Growth, Defect Formation and Morphology Control of Germanium-Silicon Semiconductor Nanowire Heterostructures. *Nano Lett.* **2011**, *11*, 4200.
(31) Houghton, D. C. Strain Relaxation Kinetics in Si1-xGex/Si Heterostructures. *J. Appl. Phys.* **1991**, *70*, 2136.
(32) Dayeh, S. A.; Mack, N. H.; Huang, J. Y.; Picraux, S. T. Advanced Core/Multi-shell Germanium/Silicon Nanowire Heterostructures: The Au-Diffusion Bottleneck. *Appl. Phys. Lett.* **2011**, *99*, 023102.
(33) Goldthorpe, I. A.; Marshall, A. F.; McIntyre, P. C. Inhibiting Strain-Induced Surface Roughening: Dislocation-Free Ge/Si and Ge/SiGe Core-Shell Nanowires. *Nano Lett.* **2009**, *9*, 3715.
(34) Zhao, Y.; Smith, J. T.; Appenzeller, J.; Yang, C. Transport Modulation in Ge/Si Core/Shell Nanowires Through Controlled Synthesis of Doped Si Shells. *Nano Lett.* **2011**, *11*, 1406.
(35) Popovitz-Biro, R.; Kretinin, A.; Huth, P. V.; Shtrikman, H. InAs/GaAs Core-Shell Nanowires. *Cryst. Growth Des.* **2011**, *11*, 3858.
(36) Dayeh, S. A.; Picraux, S. T. Direct Observation of Nanoscale Size Effects in Ge Semiconductor Nanowire Growth. *Nano Lett.* **2010**, *10*, 4032.
(37) microMegas (mM) home page project. http://zig.onera.fr/mm_home_page
(38) Liu, X. H.; Ross, F. M.; Schwarz, K. W. *Phys. Rev. Lett.* **2000**, *85*, 4088.
(39) Schwarz, K. W. *Phys. Rev. Lett.* **2003**, *91*, 145503.
(40) Grydlik, M.; Boioli, F.; Groiss, H.; Gatti, R.; Brehm, M.; Montalenti, F.; Devincre, B.; Schäffler, F.; Miglio, L. *Appl. Phys. Lett.* **2012**, *101*, 013119.